GEOPHYSICAL RESEARCH LETTERS, VOL. 36, L01603, doi:10.1029/2008GL035819, 2009

Spatial and temporal variability of biogenic gases during the Southern Ocean spring bloom

Philippe D. Tortell[1] and Matthew C. Long[2]

Received 26 August 2008; revised 16 October 2008; accepted 4 November 2008; published 6 January 2009.

[1] The Southern Ocean exerts a strong influence on global biogeochemical cycles and air-sea gas fluxes. Significant progress has been made towards understanding the general patterns of circulation and biological productivity in this region, but the small-scale dynamics of surface water gases remain poorly resolved. Here we present new data documenting unprecedented spatial and temporal variability of Southern Ocean biogenic gases during the spring phytoplankton bloom. Using real-time underway mass spectrometry, we observed significant changes in surface water O_2/Ar, pCO_2, and dimethylsulfide (DMS) concentrations over time scales of days to weeks and sub-km spatial scales. Our results demonstrate a tight coupling between physical and biological processes controlling Southern Ocean gas distributions, and highlight the distinct biogeochemical dynamics governing gas cycling in open water and ice-covered regions. **Citation:** Tortell, P. D., and M. C. Long (2009), Spatial and temporal variability of biogenic gases during the Southern Ocean spring bloom, *Geophys. Res. Lett.*, *36*, L01603, doi:10.1029/2008GL035819.

1. Introduction

[2] Global ocean surveys have identified a strong Southern Ocean sink for atmospheric CO_2 [*Takahashi et al.*, 2002], and large sources of the climate-active gas dimethylsulfide (DMS) in this region (waters south of 50°S) [*Kettle et al.*, 1999]. The distribution of these and other biogenic gases are determined by coupled biological and physical processes operating across a range of spatial and temporal scales. Surface ocean CO_2 concentrations are set by the balance between water column photosynthesis and respiration (i.e., net community production; NCP), and by physical dynamics which are sensitive to climate change [*Sarmiento et al.*, 1998]. Oceanic DMS originates from phytoplankton-derived dimethylsulfoniopropionate (DMSP), and its subsequent conversion to DMS through a variety of trophic pathways [*Stefels et al.*, 2007]. Surface water DMS concentrations are influenced by climate-sensitive variables such as mixed layer depth [*Simó and Dachs*, 2002], while atmospheric DMS can, in turn, modulate the planetary albedo through the formation of backscattering sulfate aerosols and cloud-condensation nuclei [*Charlson et al.*, 1987].

[3] Recent work has illuminated the broad-scale patterns of Southern Ocean productivity through measurements of mixed layer biological oxygen accumulation (ΔO_2/Ar) [*Reuer et al.*, 2007] and time-series analysis of remotely sensed ocean color [*Arrigo et al.*, 2008]. Iron and/or light limitation restricts phytoplankton growth over much of the region [*Boyd*, 2002], but mesoscale Fe fertilization can occur where frontal boundaries interact with deep sea bathymetric features [*Debaar et al.*, 1995; *Sokolov and Rintoul*, 2007] and in seasonal ice zones [*Sedwick and DiTullio*, 1997]. Particularly high rates of primary productivity are observed in coastal Antarctic polynyas such as the Ross Sea [*Arrigo et al.*, 2008], and field programs have documented extreme spatial and temporal variability in these regions [*Hales and Takahashi*, 2004].

[4] With the exception of CO_2, the fine-scale (<10–100 Km) distribution and variability of Southern Ocean gases remain poorly described, particularly in ice-covered regions. Here we present a new data set of Southern Ocean CO_2, O_2/Ar and DMS distributions obtained with ship-board mass spectrometry. Results obtained from two meridional transects demonstrate unprecedented spatial variability in surface water biogenic gases, and a rapid evolution from winter to summer-time regimes during the initiation of the spring phytoplankton bloom. Spatial analysis of gas distributions demonstrates significantly different scales of variability in open water and ice covered zones, providing insight into the underlying physical and biogeochemical processes driving gas dynamics in these contrasting regions.

2. Methods

[5] Underway data were collected on the RVIB Nathaniel B. Palmer (cruise NPB06-08) as part of the Controls on Ross Sea Algal Community Structure (CORSACS) program. Measurements were made on a transit from New Zealand to the Ross Sea polynya between Nov. 2 and Nov. 12, 2006 and on the return transit from Dec. 2 to Dec. 10, 2006. The southbound and northbound transects sampled the region between 177°E and 173°W from 53° to 75°S, and overlapped within <2° longitude over a time interval of 20–37 days.

[6] Dissolved gas analysis was conducted using membrane inlet mass spectrometry as described previously [*Gueguen and Tortell*, 2008]. Briefly, surface seawater from the ship's intake system (~5 m depth) was pumped through a sampling cuvette and gases extracted through a silicone membrane into the ion source of a quadropole mass spectrometer for continuous flow analysis. Ion current measurements of CO_2, O_2, Ar, and DMS were calibrated to absolute concentrations for CO_2 and DMS, and an atmospheric saturation ratio, ΔO_2/Ar, following *Gueguen and Tortell* [2008]. As defined in previous studies [*Craig and Hayward*,

[1]Department of Earth and Ocean Sciences and Department of Botany, University of British Columbia, Vancouver, British Columbia, Canada.
[2]Department of Environmental Earth System Sciences, Stanford University, Stanford, California, USA.

0094-8276/09/2008GL035819$05.00

1987], $\Delta O_2/Ar$ represents biological O_2 saturation which is largely insensitive to physical processes such as warming, bubble injection, and atmospheric pressure changes. During underway analysis, gas concentrations were measured every ~30 seconds (mean spatial resolution of ~50 to 300 m), and averaged into one minute temporal bins for alignment with temperature, salinity and chlorophyll *a* fluorescence measurements obtained from the ship's underway sensors.

[7] Daily sea-ice concentrations were derived from Advanced Microwave Scanning Radiometer - Earth Observing System (AMSR-E) data, gridded at 12.5 × 12.5 km resolution [*Cavalieri and Comiso*, 2004]. The sea-ice zone (SIZ) was defined as the region south of the transition between open water and ice covered regions (>10% coverage) at ~64.5°S. Chlorophyll *a* concentrations were obtained from 8-day mean SeaWiFS imagery (http://oceancolor.gsfc.nasa.gov/cgi/level3.pl). We calculated biologically-induced air-sea O_2 fluxes from mixed layer $\Delta O_2/Ar$ data using the methodology of *Reuer et al.* [2007], in conjunction with NCEP/NCAR reanalysis wind speed data [*Kalnay et al.*, 1996] and the piston velocity parameterization of *Wanninkhof* [1992]. Under the assumption of steady-state productivity and minimal vertical exchange across the base of the mixed layer, calculated O_2 fluxes provide an estimate of net community production (NCP) over the characteristic residence time of mixed layer O_2. Wind speed and mixed layer depth data are used to derive a time-dependent weighting function for daily piston velocities based on fraction of the mixed layer ventilated on any given day [*Reuer et al.*, 2007]. We obtained mixed layer estimates (defined as a 0.125 change in σ_θ) from the global climatology of Samuels and Cox, available through the National Center for Atmospheric Research (www.dss.ucar.edu/data). Uncertainty in the mixed layer depths affects the relative weighting of daily piston velocity values, but the resulting potential errors in NCP calculations are small compared to those associated with the wind speed-dependent parameterization of piston velocities [see *Reuer et al.*, 2007].

[8] We quantified the spatial variability of gases and hydrographic parameters using a semivariogram analysis which examines variance as a function of the lag distance separating samples [*Doney et al.*, 2003]. The empirical semivariogram is defined as the sum of squared deviations at a particular lag distance, normalized by twice the number of data points separated by that distance. We calculated the value of this function across a range of lag distances, and fit the resulting curves with a spherical model describing the increase in sample variance, V_d, with increasing lag distance, d:

$$V_d = c_o + (\sigma^2 - c_o) * \left(3/2 * d/r - 0.5 * (d/r)^3\right) \quad (1)$$

The y intercept, or 'nugget' (c_o), represents the amount of unresolved variance at spatial scales below the sampling resolution, while σ^2 approximates the maximum variance of the data. The parameter r is the characteristic length scale ('range') representing the distance beyond which samples become uncorrelated. We derived least-squares estimates and standard errors for c_o, σ^2 and r for open water and SIZ transects using a Marquardt-Levenberg non-linear regression algorithm. Prior to analysis, transect data were interpolated to a regular sampling interval of 0.25 Km, and temperature data from the open water region were linearly detrended to remove the strong meridional gradient.

3. Results

[9] Our sampling transects coincided with the initiation of Southern Ocean phytoplankton blooms in both open waters and the SIZ. SeaWiFS imagery revealed chlorophyll *a* concentrations of up to ~1 μg L^{-1} north of the SIZ (Figure 1a), similar to previous observations in the same study region [*Moore et al.*, 1999]. Analysis of the 10 year SeaWiFS record (zonal-mean from 176°E – 172°W) indicates that this early spring bloom is a consistent feature of our study area. Typical dynamics of bloom initiation in the SIZ are less certain since ocean color measurements are not available for heavily ice covered regions. However, our underway chlorophyll *a* fluorescence measurements (Figure 1b) indicated the rapid development of large, but highly localized phytoplankton blooms within the pack ice (~70°S) and at the northern edge of the Ross Sea polynya (~74°S). Sea ice concentrations decreased substantially in both of these regions during the interval between our two survey transits.

[10] The open water phytoplankton bloom was associated with significant hydrographic changes in the upper water column, coupled to increasing day length and solar irradiance during the early spring season. In the time between our southbound and northbound transits, surface water temperature increased by up to 2°C north of ~64°S (Figure 1c) and climatological mixed layers show significant shoaling in the open ocean region (from 160 ± 78 m to 62 ± 14 m). In contrast, sea surface temperature and climatological mixed layer depths demonstrated much smaller temporal variability in the SIZ. The dominant hydrographic change in this region was a significant decrease in ice cover. The decrease in percent ice cover was highly correlated to the small temperature increases observed in the SIZ (Pearson correlation, $r = 0.66$, $p < 0.001$).

[11] Significant changes in biogenic gas distributions were coupled with increased phytoplankton biomass across our entire survey region. On the pre-bloom southbound transit through open ocean waters, mean $\Delta O_2/Ar$ and pCO_2 were close to atmospheric equilibrium in the open water region (0.64% and 375 ppm, respectively, Figures 1d and 1e), and NCP derived from biologically induced air-sea O_2 fluxes ranged from ~−5 to + 40 mmol m^{-2} d^{-1} (Figure 1d, inset). On the northbound return transit, open water $\Delta O_2/Ar$ increased by a mean value of 1.7% (range −0.9 to 4%), while NCP ranged from ~20–70 mmol m^{-2} d^{-1}. Increased biological activity on the northbound transect was also evident in significant pCO_2 drawdown and DMS accumulation. On average, pCO_2 decreased by 15 μatm in the open water region, with a maximum drawdown of >30 μatm at some locations. Concentrations of DMS more than doubled north of 64°S, with a mean increase of ~2 nM. The accumulation of O_2 was highly correlated to pCO_2 drawdown and, to a lesser extent, with chlorophyll *a* increases north of the SIZ (Table 1). In contrast, DMS accumulation showed a weak (but statistically significant) positive correlation with CO_2 drawdown in this region, but no statistically significant relationship with chlorophyll *a* or $\Delta O_2/Ar$ increases (Table 1).

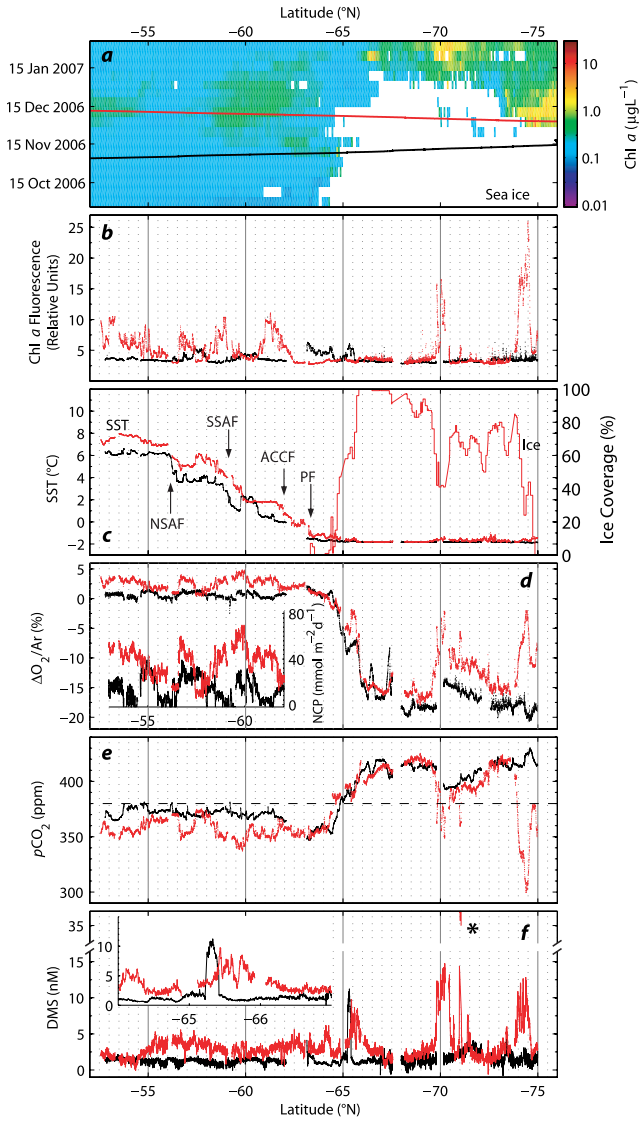

Figure 1. Surface water property distributions along two Southern Ocean transects, Nov.–Dec. 2006. Chlorophyll *a* concentrations were derived from (a) SeaWiFS 8-day mean composite data and (b) ship-based underway fluorometric analysis. Black and red lines on panel Figure 1a show the ship's position on the southbound and northbound transits, respectively, while white areas denote the presence of sea ice or cloud cover. Black symbols show results from the Southward transect, while red symbols show the Northward transect data. (c) Arrows show the approximate positions of the Northern Sub-Antarctic Front (NSAF), Southern Sub-Antarctic Front (SSAF), Polar Front (PF) and Southern Antarctic Circumpolar Current Front (ACCF) as defined by [*Budillon and Rintoul*, 2003]. (d, inset) Net community production derived from biologically-induced O_2 fluxes (mmol m^{-2} d^{-1}) for the region north of 63°S. (e) Dashed horizontal line shows the current atmospheric pCO_2 level (~380 ppm). (f, inset) Greater detail for the latitudinal range indicated, while the asterisk highlights a region of particularly intense DMS accumulation.

[12] Dissolved gas distributions in the SIZ displayed significantly greater spatial and temporal heterogeneity than in the open ocean. On both southbound and northbound sampling transects, sharp gradients in O_2/Ar and pCO_2 existed across the transition from open water to the SIZ (~64°–66°S), accompanied by significant DMS accumulation (Figure 1f, inset). During our initial survey, ΔO_2/Ar was strongly undersaturated (<−20%) south of 65° (Figure 1d), while pCO_2 exceeded atmospheric equilibrium by up to 60 ppm (Figure 1e). Elevated pCO_2 reflects deep water convection and net winter time respiration under the sea ice, and potentially, CO_2 rejection during sea ice formation [*Nomura et al.*, 2006].

[13] A significant increase in biological oxygen saturation indicated the onset of net autotrophic production in the SIZ. In the interval between our southbound and northbound surveys, ΔO_2/Ar increased by an average value of 3.6%, with particularly large increases (up to 17%) associated with elevated chlorophyll *a* fluorescence at ~70° and 74°S. Net productivity was observed even in regions with persistent ice cover (>80%) where there was no detectable increase in surface water chlorophyll *a* levels. This result suggests a significant contribution of ice algae to water column productivity. The mean pCO_2 drawdown in the SIZ (16 ppm) was similar to the open water region, but drawdown as high as ~120 ppm was observed at the northern boundary of the Ross Sea polynya (~74°S). DMS showed significant accumulation (>10 nM) at the boundaries of the SIZ (~64° and 74°S) and in regions of ice retreat within the ice pack (71° and 71.5°) (Figure 1f). The DMS 'hot-spot' at ~71.5°S (highlighted on Figure 1f) was particularly noteworthy for its high concentration and small spatial scale. Concentrations increased from <3 nM to ~40 nM over a spatial scale of <5 Km, coincident with an increase in chlorophyll *a* fluorescence and ΔO_2/Ar, and a drawdown of pCO_2. This feature highlights the extreme spatial heterogeneity of DMS concentrations in the SIZ. Across the entire SIZ, increased O_2/Ar was highly correlated to pCO_2 drawdown and chlorophyll *a* increases (Table 1) indicating that biological activity rather than physical effects (e.g. melt water dilution) exerted a dominant control on CO_2 and O_2 distributions in the SIZ. DMS accumulation was also coupled to biological activity as judged by statistically significant correlations with O_2/Ar and chlorophyll *a* increases and pCO_2 drawdown (Table 1).

Table 1. Pearson Correlation Coefficients for Parameters in Open Water and Ice-Covered Regions[a]

	SST	Chl *a*	pCO_2	ΔO_2/Ar
Chl *a*	.37[b]/.23[c]			
pCO_2	ns[d]/−.41[e]	−.54[e]/−.89[e]		
ΔO_2/Ar	ns[d]/.50[e]	.62[e]/.77[e]	−.88[e]/−.90[e]	
DMS	.33[b]/.18[c]	ns[d]/.50[e]	.30[b]/−.52[d]	ns[d]/.48[e]

[a]Time-normalized rates of change were computed for each parameter (i.e., Δ parameter/Δ time) and averaged into 0.1° zonal bins. The first and second entries for each cell show the correlation coefficients for these temporal parameter changes in open water (n = 74) and the sea-ice zone (n = 81), respectively.
[b]$p < 0.005$.
[c]$p < 0.05$.
[d]$p > 0.05$; not statistically significant.
[e]$p < .0001$.

[14] Semivariogram analysis demonstrated significant differences in spatial variability among all parameters in open waters and the SIZ (Figure 2). Temperature showed greater variability in the open water region, likely due to the presence of strong frontal boundaries between 55 and 65°S, and the thermal inertial effects of ice in the SIZ. In contrast, chlorophyll *a* and all gases showed significantly greater spatial heterogeneity in the SIZ, with σ^2 values up to 4.5 fold higher than in the open water region. Characteristic length scales (r) varied between 70 and 326 Km. Length scales were slightly smaller in the open water region for temperature and CO_2, but larger for chlorophyll *a*, $\Delta O_2/Ar$ and DMS. For most parameters, spherical model fits were unable to accurately capture the true nugget value (c_o) owing to a steep initial rise in variance at length scales <10 Km (see DMS, Figure 2e). We thus estimated the nugget values using the mean standard deviation computed at the smallest length scale of our observations (0.25 Km). On average, nugget values were <10% of the σ^2 values, indicating that our observations resolved nearly all of the variability in the measured variables.

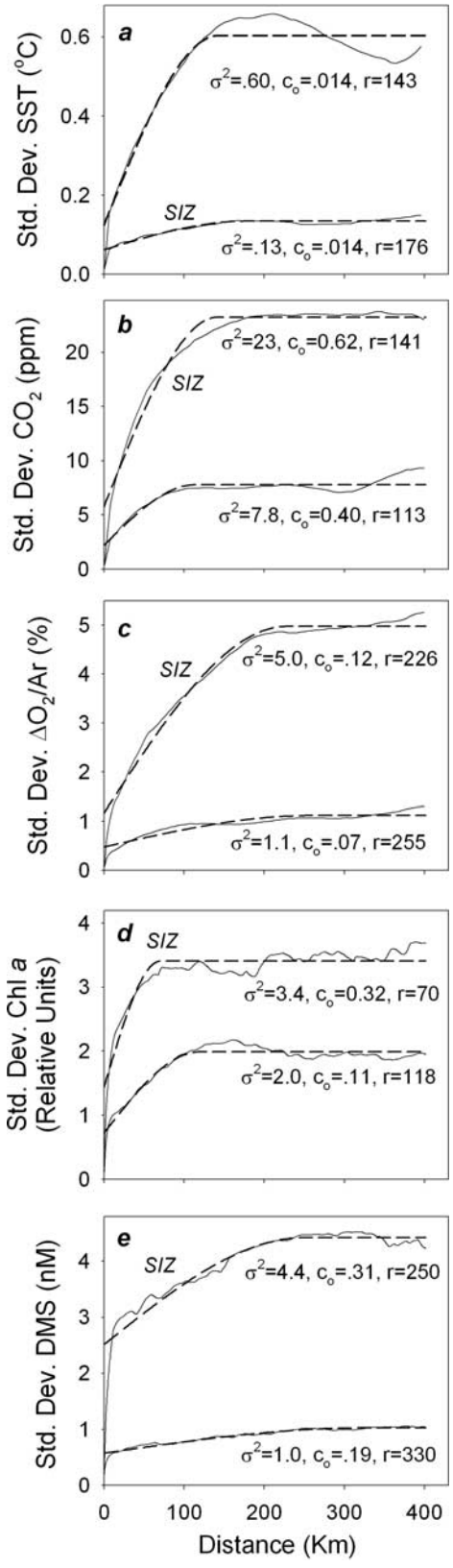

Figure 2. Spatial semivariograms for chlorophyll *a*, sea-surface temperature and gases along the northbound transect in open waters and the SIZ (labeled on figure). Solid thin lines represent the computed standard deviation for each parameter over a range of sampling lag distances. Thicker dashed lines show the best-fit regression equations for the spherical model with parameter estimates given below each curve. See methods for additional details of the model fits and parameter values.

4. Discussion and Conclusions

[15] Recent analysis of remotely sensed global ocean color [*Doney et al.*, 2003] has demonstrated that sub-mesocale variability (i.e. <10 Km) dominates over much of the oligotrophic ocean, and contributes significantly (up to 30%) to the total variability of high productivity regions. This sub-mesoscale structure is not well represented in many remote sensing data products, and cannot be adequately resolved with discrete hydrographic sampling. By comparison, our high resolution ship-board analysis captured more than 90% of the total spatial variance in net community production and biogenic gas distributions in the Southern Ocean.

[16] Resolution of sub-mesoscale gas distributions provides insight into the underlying biogeochemical dynamics which drive surface ocean variability. In the open water region north of the SIZ, frontal boundaries appear to be an important mechanism affecting gas distributions, as evidenced by the sharp changes in biological oxygen fluxes ($\sim$10–70 mmol m^{-2} d^{-1}) we observed across the northern and southern Sub-Antarctic fronts (56°–60°S) and, to a lesser extent, across the Polar Front ($\sim$62°S). Previous large-scale surveys have identified a meriodional NCP gradient in the Southern Ocean [*Reuer et al.*, 2007] and this has been attributed to the geographic pattern of aeolian Fe fluxes [*Cassar et al.*, 2007]. Our results suggest that sub-mesoscale mixing processes may drive equally large local gradients of NCP and other biogenic gases during the early spring-time growing season.

[17] In the SIZ, increased biological activity and gas cycling appears tightly coupled to ice melt during the early growing season. Ice melt can stimulate biological activity in underlying waters by enhancing vertical stratification [*Mitchell and Holm-Hansen*, 1991], and/or through Fe fertilization [*Sedwick and DiTullio*, 1997]. In addition,

previous work has suggested that significant gas cycling may occur in the sea ice itself [*Delille et al.*, 2007]. It is presently unclear to what extent ice covered regions may be a net source or sink of various biogenic gases, since these regions are chronically under-sampled with respect to their potential spatial and temporal variability. The Antarctic SIZ is a potential source of CO_2 to the atmosphere due the accumulation of high winter-time pCO_2 [*Bakker et al.*, 1997]. Our results demonstrate, however, that intense pCO_2 undersaturation can develop in the short interval following ice retreat, limiting early season CO_2 efflux. The high DMS concentrations we observed in the SIZ are consistent with recent field observations [*Delille et al.*, 2007; *Kiene et al.*, 2007], and suggest that sea-ice communities play an important role in Antarctic DMS production. More extensive surveys will be needed to characterize the abundance and persistence of DMS 'hot-spots' in the SIZ and their quantitative influence on regional air-sea fluxes.

[18] The distribution of biogenic gases we observed south of New Zealand may be representative of the broader Southern Ocean, given the similarity in phytoplankton productivity and sea-ice dynamics across Antarctic subregions [*Arrigo et al.*, 2008]. Our results thus have implications for understanding regional biogeochemical budgets, particularly in terms of quantifying net annual air-sea flux of biogenic gases and the relative contribution of the SIZ to Southern Ocean productivity. These research questions are particularly pressing in light of possible decreases in Antarctic sea-ice cover over the coming century [*Curran et al.*, 2003] and predicted changes in SIZ gas fluxes under various global warming scenarios [*Gabric et al.*, 2003].

[19] **Acknowledgments.** This work was supported by the US NSF (OPP 0338350), and funding from NSERC (PDT). We wish to thank Christopher Payne for expert technical support at sea, and the Captain and crew of the RVIB Nathanial B. Palmer for logistical assistance. Michael Bender, Kevin Arrigo and two anonymous reviewers provided constructive criticisms on earlier versions of the manuscript.

References

Arrigo, K. R., G. L. van Dijken, and S. Bushinsky (2008), Primary production in the Southern Ocean, 1997–2006, *J. Geophys. Res.*, *113*, C08004, doi:10.1029/2007JC004551.

Bakker, D. C. E., et al. (1997), Changes of carbon dioxide in surface waters during spring in the Southern Ocean, *Deep Sea Res., Part II*, *44*(1–2), 91–127.

Boyd, P. W. (2002), Environmental factors controlling phytoplankton processes in the Southern Ocean, *J. Phycol.*, *38*(5), 844–861.

Budillon, G., and S. R. Rintoul (2003), Fronts and upper ocean thermal variability south of New Zealand, *Antarct. Sci.*, *15*(1), 141–152.

Cassar, N., et al. (2007), The Southern Ocean biological response to Aeolian iron deposition, *Science*, *317*(5841), 1067–1070.

Cavalieri, D., and J. Comiso (2004), AMSR-E/Aqua daily L3 12.5 km Brightness Temperature, Sea Ice Concentration, and Snow Depth Polar Grids V001, March to June 2004, http://nsidc.org/data/docs/daac/ae_si12_12km_tb_sea_ice_and_snow.gd.html, Natl. Snow and Ice Data Cent., Boulder, Colo. (Updated daily.)

Charlson, R. J., et al. (1987), Oceanic phytoplankton, atmospheric sulfur, cloud albedo and climate, *Nature*, *326*(6114), 655–661.

Craig, H., and T. Hayward (1987), Oxygen supersaturation in the ocean: Biological versus physical contributions, *Science*, *235*(4785), 199–202.

Curran, M. A. J., et al. (2003), Ice core evidence for Antarctic sea ice decline since the 1950s, *Science*, *302*(5648), 1203–1206, doi:10.1126/science.1087888.

Debaar, H. J. W., et al. (1995), Importance of iron for plankton blooms and carbon dioxide drawdown in the Southern Ocean, *Nature*, *373*(6513), 412–415.

Delille, B., et al. (2007), Biogas (CO_2, O_2, dimethylsulfide) dynamics in spring Antarctic fast ice, *Limnol. Oceanogr.*, *52*(4), 1367–1379.

Doney, S. C., D. M. Glover, S. J. McCue, and M. Fuentes (2003), Mesoscale variability of Sea-viewing Wide Field-of-view Sensor (SeaWiFS) satellite ocean color: Global patterns and spatial scales, *J. Geophys. Res.*, *108*(C2), 3024, doi:10.1029/2001JC000843.

Gabric, A. J., et al. (2003), The sensitivity of dimethyl sulfide production to simulated climate changed in the eastern Antarctic Southern Ocean, *Tellus, Ser. B*, *55*(5), 966–981.

Gueguen, C., and P. D. Tortell (2008), High-resolution measurement of Southern Ocean CO_2 and O_2/Ar by membrane inlet mass spectrometry, *Mar. Chem.*, *108*(3–4), 184–194.

Hales, B., and T. Takahashi (2004), High-resolution biogeochemical investigation of the Ross Sea, Antarctica, during the AESOPS (U. S. JGOFS) Program, *Global Biogeochem. Cycles*, *18*, GB3006, doi:10.1029/2003GB002165.

Kalnay, E., et al. (1996), The NCEP/NCAR 40-year reanalysis project, *Bull. Am. Meteorol. Soc.*, *77*(3), 437–471.

Kettle, A. J., et al. (1999), A global database of sea surface dimethylsulfide (DMS) measurements and a procedure to predict sea surface DMS as a function of latitude, longitude, and month, *Global Biogeochem. Cycles*, *13*(2), 399–444.

Kiene, R. P., et al. (2007), Distribution and cycling of dimethylsulfide, dimethylsulfoniopropionate, and dimethylsulfoxide during spring and early summer in the Southern Ocean south of New Zealand, *Aquat. Sci.*, *69*(3), 305–319.

Mitchell, B. G., and O. Holm-Hansen (1991), Bio-optical properties of Antarctic Peninsula waters: Differentiation from temperate ocean models, *Deep Sea Res., Part A*, *38*, 1009–1028.

Moore, J. K., M. R. Abbott, J. G. Richman, W. O. Smith, T. J. Cowles, K. H. Coale, W. D. Gardner, and R. T. Barber (1999), SeaWiFS satellite ocean color data from the Southern Ocean, *Geophys. Res. Lett.*, *26*(10), 1465–1468.

Nomura, D., et al. (2006), The effect of sea-ice growth on air-sea CO_2 flux in a tank experiment, *Tellus, Ser. B*, *58*(5), 418–426.

Reuer, M. K., et al. (2007), New estimates of Southern Ocean biological production rates from O_2/Ar ratios and the triple isotope composition of O_2, *Deep Sea Res., Part I*, *54*(6), 951–974.

Sarmiento, J. L., et al. (1998), Simulated response of the ocean carbon cycle to anthropogenic climate warming, *Nature*, *393*(6682), 245–249.

Sedwick, P. N., and G. R. DiTullio (1997), Regulation of algal blooms in Antarctic shelf waters by the release of iron from melting sea ice, *Geophys. Res. Lett.*, *24*(20), 2515–2518.

Simó, R., and J. Dachs (2002), Global ocean emission of dimethylsulfide predicted from biogeophysical data, *Global Biogeochem. Cycles*, *16*(4), 1018, doi:10.1029/2001GB001829.

Sokolov, S., and S. R. Rintoul (2007), On the relationship between fronts of the Antarctic Circumpolar Current and surface chlorophyll concentrations in the Southern Ocean, *J. Geophys. Res.*, *112*, C07030, doi:10.1029/2006JC004072.

Stefels, J., et al. (2007), Environmental constraints on the production and removal of the climatically active gas dimethylsulphide (DMS) and implications for ecosystem modelling, *Biogeochemistry*, *83*(1–3), 245–275.

Takahashi, T., et al. (2002), Global sea-air CO_2 flux based on climatological surface ocean pCO_2, and seasonal biological and temperature effects, *Deep Sea Res., Part II*, *49*(9–10), 1601–1622.

Wanninkhof, R. (1992), Relationship between wind speed and gas exchange over the ocean, *J. Geophys. Res.*, *97*(C5), 7373–7382.

M. C. Long, Department of Environmental Earth System Sciences, Stanford University, Braun Hall, Building 320, Stanford, CA 94305-2115, USA.

P. D. Tortell, Department of Earth and Ocean Sciences, University of British Columbia, 6270 University Boulevard, Vancouver, BC V6T 1Z4, Canada. (ptortell@eos.ubc.ca)